Assessing Transducer Parameters for Accurate Medium Sound Speed Estimation and Image Reconstruction

Waasdorp, Rick; Maresca, David; Renaud, Guillaume

DOI
10.1109/TUFFC.2024.3445131

Publication date
2024

Document Version
Final published version

Published in
IEEE Transactions on Ultrasonics, Ferroelectrics, and Frequency Control

Assessing Transducer Parameters for Accurate Medium Sound Speed Estimation and Image Reconstruction

Rick Waasdorp, David Maresca, and Guillaume Renaud

***Abstract*—The influence of the transducer lens on image reconstruction is often overlooked. Lenses usually exhibit a lower sound speed than soft biological tissues. In academic research, the exact lens sound speed and thickness are typically unknown. Here, we present a simple and nondestructive method to characterize the lens sound speed and thickness as well as the time to peak of the round-trip ultrasound waveform, another key parameter for optimal image reconstruction. We applied our method to three transducers with center frequencies of 2.5, 7.5, and 15 MHz. We estimated the three parameters with an element-by-element transmission sequence that records internal reflections within the lens. We validated the retrieved parameters using an autofocusing approach that estimates sound speed in water. We show that the combination of our parameters estimation method with two-layer ray tracing outperforms standard image reconstruction. For all transducers, we successfully improved the accuracy of medium sound speed estimation, spatial resolution, and contrast. The proposed method is simple and robust and provides an accurate estimation of the transducer lens parameters and the time to peak of the ultrasound waveform, which leads to improved ultrasound image quality.**

***Index Terms*—Aberration correction, lens, ray tracing, sound speed estimation, transducer, ultrasound.**

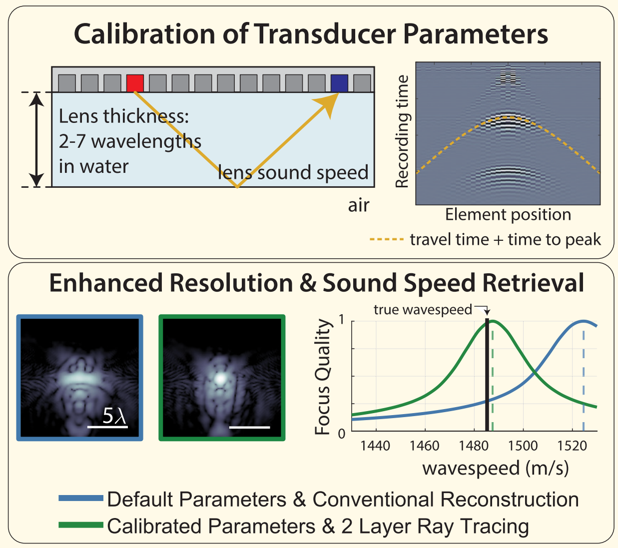

I. Introduction

DELAY-AND-SUM (DAS) is the most common technique for medical ultrasound image reconstruction [1]. In DAS, the recorded echo signals are summed along the estimated round-trip travel times from the transmit subaperture to the image pixel and back to the receive subaperture. The pulse-echo travel time can be divided into three components: the travel time in the transducer lens, the travel time in the scanned medium, and the time to peak of the round-trip ultrasound waveform. Because these three components are rarely accurately known, DAS is often applied using approximated travel times, which leads to suboptimal image resolution and contrast.

The travel time through the transducer lens depends on the geometry and acoustic properties of the lens, i.e., the sound speed and thickness of the lens. However, transducer manufacturers rarely report accurate values for the lens sound speed and thickness. Instead, a lens travel time correction $t_{\text{lens cor}}$ is often reported to account for the difference in sound speed in the lens and the scanned medium [1]. A transducer lens is usually made of silicone rubber and its sound speed is lower than that of soft tissue ($c_{\text{lens}} \approx 1000$ m/s [2] versus $c_{\text{soft tissue}} \approx 1540$ m/s). The lens thickness typically measures 2–7 ultrasound wavelengths (λ) in water. Lenses are typically used to focus the ultrasound beam in the elevation direction for 1-D arrays. Recent advances in acoustic lenses for 2-D arrays show that 2-D arrays where each element has its own diverging lens lead to increased sensitivity and focusing capabilities [3]. Due to the different sound speed in the lens and the scanned medium, an ultrasound ray between a transducer element and a point in the scanned medium is refracted. Modeling the travel time through the lens as a

Manuscript received 24 May 2024; accepted 13 August 2024. Date of publication 27 August 2024; date of current version 10 October 2024. This work was supported by the Medical Delta Consortium through the Ultrafast Heart and Brain Program, a collaboration between Delft University of Technology, Leiden University, Erasmus University Rotterdam, Leiden University Medical Center, and Erasmus Medical Centre. *(Corresponding author: Guillaume Renaud.)*

The authors are with the Department of Imaging Physics, Delft University of Technology, 2628 CJ Delft, The Netherlands (e-mail: g.g.j.renaud@tudelft.nl).

Digital Object Identifier 10.1109/TUFFC.2024.3445131

Highlights

- **We propose a simple nondestructive method to accurately determine the time to peak of the backscattered ultrasound pulse, the transducer lens thickness, and the lens speed of sound.**
- **Using the estimated transducer parameters with a two-layer ray-tracing reconstruction approach enables accurate medium speed of sound retrieval and improves image resolution and contrast.**
- **Calibrated transducer parameters together with a two-layer ray-tracing reconstruction approach lead to significant improvements in the near field up to a depth of 100 ultrasound wavelengths.**

time offset neglects the dependence of the traveling distance in the lens on the ultrasound ray angle and ignores wave refraction at the interface between the lens and the scanned medium.

Ultrasound scanners typically transmit short sine bursts with few cycles of vibration at the center frequency of the ultrasound probe. For accurate image reconstruction, it is important to account for a delay equal to the time to peak (t_{ttp}) of the received imaging waveform envelope [Fig. 1(a)]. The time to peak is usually estimated based on a simulated waveform using the convolution of the two-way impulse response of a transducer and the driving electrical signal. However, such simulated backscattered waveforms do not always exactly resemble the experimentally received pulse due to inaccurate knowledge of the transmit and receive impulse responses and the driving electrical signal. An inaccurate time to peak leads to an additional source of error for the delays used in DAS.

To the best of our knowledge, no nondestructive method to estimate the transducer parameters has been reported. Gray and Coussios [4] proposed a method to characterize the lens parameters by partially cutting away the silicone rubber lens and interrogating the imaging transducer with a focused transducer in a calibration setup. By comparing the arrival times of the focused transmit for the cutaway section and the intact section, they could assess the lens thickness and sound speed. However, the time to peak could not be assessed using this method.

Here, we present a simple nondestructive method that enables accurate estimation of the lens thickness, the lens sound speed, and the time to peak of the backscattered imaging waveform. The method leverages internal lens reflections recorded using a synthetic aperture imaging sequence with single-element transmissions [5] and does not require any calibration setup. We validated our method with numerically generated echo signals and experimentally by estimating the sound speed in water with a known speed of sound, using an autofocusing method [6], [7], [8], [9], [10], [11]. Finally, we demonstrate that the accurate estimation of transducer parameters leads to improved ultrasound imaging resolution and contrast, using thin wires immersed in water.

The MATLAB (MathWorks Inc., Natick, MA, USA) code to estimate transducer parameters and example data for two transducers is available on GitHub https://github.com/MarescaRenaudLabs/ProbeParameterEstimation.

TABLE I
OVERVIEW OF TRANSDUCER PROPERTIES OF USED TRANSDUCERS

	P4-1	**L12-3v**	**L6-24D**
Array Type	Phased	Linear	Linear
Pitch (mm)	0.295	0.200	0.135
Center frequency (MHz)	2.5	7.5	15
Number of elements	96	192	192
Elevation focus depth (mm)	80	20	12
Transmit Frequency (MHz)	2.5	8.93	15.625
Default Parameters			
Time to peak $t_{\mathrm{ttp,m}}$ (µs)	0.83	0.22	-
Lens correction $t_{\mathrm{lens\ cor,m}}$ (µs)	3.33	1.60	-

II. METHODS

A. Calibrating Transducer Parameters

1) Experimental Data Acquisition: We characterized the lens properties of three ultrasound transducers with different frequencies and pitches, including a 2.5-MHz phased-array transducer (P4-1 ATL/Philips, Bothell, WA, USA), a 7.5-MHz linear array transducer (L12-3v, Verasonics Inc., Kirkland, WA, USA), and a 15-MHz linear array transducer (L6-24D, GE Healthcare, Frankfurt, Germany). An overview of transducer specifications is provided in Table I. All experimental data acquisition was performed with a programmable ultrasound imaging system (Vantage, Verasonics Inc., Kirkland, WA, USA).

To calibrate the acoustic and geometric lens properties and the time to peak of the ultrasound waveform, we record the internal lens reflections, while the probe is coupled with air. We used a synthetic aperture imaging sequence [5] with single-element transmissions and recorded with all elements [Fig. 1(b)]. Each single element is electrically excited with a one-cycle signal at the center frequency. The sampling frequency of the recorded echo signals was equal to four times the ultrasound center frequency. To avoid overheating the transducer arrays, acquisitions in air were done at a low pulse repetition frequency of 100 Hz. The received data were averaged 200 times to improve the signal-to-noise ratio of internal lens reflections.

Next, we combined multiple single-element transmits into one averaged dataset. We selected subapertures of an odd number of elements N_b. For a transducer with N_e elements, we define $N_e - N_b + 1$ symmetric subapertures that could be averaged. The resulting averaged echo signals are shown in

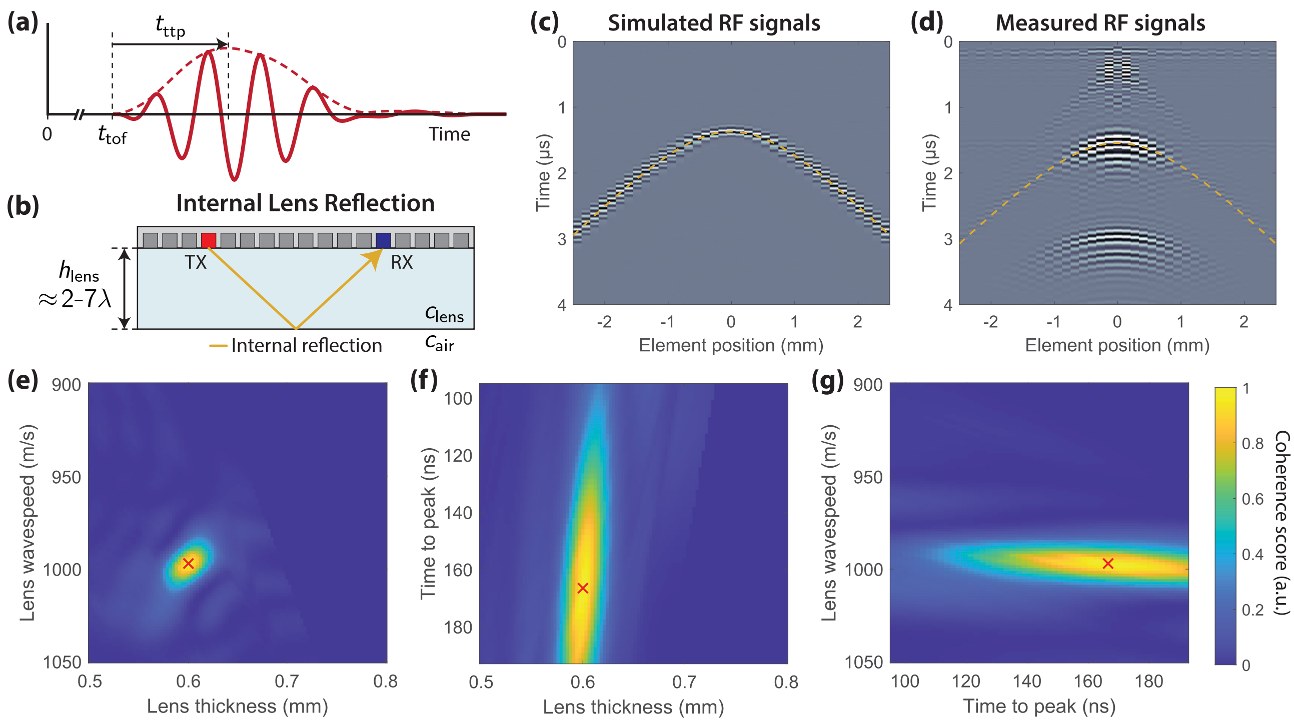

Fig. 1. (a) At time $t = 0$, the transducer emits a short ultrasound pulse, and the scanner starts to record echo signals. In the recorded echo signals (red solid line), the time to peak corresponds to the max in the envelope of the echo signals (red dashed line). (b) Schematic representation of the internal lens reflection when firing the transducer in air. The lens thickness typically corresponds to 2–7 ultrasound wavelengths (λ) in water. (c) Simulated internal lens reflection echo signals using a modeled L6-24D transducer. Dashed line indicates the calculated arrival time of the envelope peak, calculated using the estimated transducer parameters. (d) Measured echo signals from internal lens reflection with an L6-24D transducer firing in air. Dashed line indicates the calculated arrival time of the envelope peak, calculated using the estimated transducer parameters. The signal recorded after 3 µs is a secondary reflection. (e)–(g) Normalized coherence of the numerically generated echo signals (c) along the arrival time hyperbolas for different tested values for lens thickness, lens sound speed, and time to peak. The estimated transducer parameters are indicated by the red cross.

Fig. 1(d). In the present study, we used N_b between 41 and 51 for all transducers.

2) Estimation of Transducer Parameters: We estimated the lens sound speed $\hat{c}_{\text{lens}}$, lens thickness $\hat{h}_{\text{lens}}$, and time to peak $\hat{t}_{\text{ttp}}$ of the transducer with a grid search approach by computing the arrival times for the first internal reflection and maximizing the coherence of the echo signals across receive channels. When the correct lens sound speed c_{lens}, lens thickness h_{lens}, and waveform time to peak t_{ttp} are used the calculated arrival time, hyperbolas of the internal reflection will match the peak envelope of the measured echoes and lead to maximum coherence.

We define the analytic echo signal for receiving element i as s_i obtained by the Hilbert transform of the averaged echo data. The round-trip travel time $\tau_{\text{rt},i}$ for the primary reflection in the lens is given by the following equation:

$$\tau_{\text{rt}}(\Delta x_i) = \frac{2}{c_{\text{lens}}}\sqrt{\left(\frac{\Delta x_i}{2}\right)^2 + {h_{\text{lens}}}^2} \tag{1}$$

with $\Delta x_i = x_{\text{tx},i} - x_{\text{rx},i}$ the lateral distance between the transmitting and receiving element. Then, the arrival time hyperbola τ_i is obtained by adding the time to peak t_{ttp} to the round-trip travel time τ_{rt} ($\tau_i = t_{\text{ttp}} + \tau_{\text{rt}}$). Then, we compute the coherence weighted by the signal power C_w as follows:

$$C_w = \left|\sum_{i=1}^{N_b} \frac{s_i(\tau_i)}{|s_i(\tau_i)|}\right|^2 \sum_{i=1}^{N_b} |s_i(\tau_i)|^2. \tag{2}$$

During the grid search, we compute the coherence C_w for all tested values for lens sound speed c_{lens}, lens thickness h_{lens}, and the time to peak t_{ttp}. The lens sound speed was varied from 900 to 1100 m/s, considering that the wave speed of silicone rubber is around 1000 m/s [2]. The lens thickness was varied from two to seven ultrasound wavelengths (in water), and the time to peak was varied from $(N_c/f_c) - (1/f_c)$ to $(N_c/f_c) + (4/f_c)$, with f_c the transducer center frequency and N_c the number of cycles in transmit.

3) Numerical Simulation of Internal Transducer Lens Reflections: To validate the method to calibrate transducer parameters, we simulated an L6-24D transducer with the numerical wave solver k-Wave [13], which consists of 128 elements with a pitch of 0.135 mm. The lens was modeled as a 0.6-mm-thick layer of silicone rubber with a sound speed of 1000 m/s and a density of $1000\,\text{kg/m}^3$ [2]. Below the lens, a layer of air-mimicking material was modeled with a sound speed of 341 m/s and a density of $600\,\text{kg/m}^3$. Note that the density was chosen higher than the actual density of air ($1.2\,\text{kg/m}^3$) to avoid numerical instabilities in the simulation.

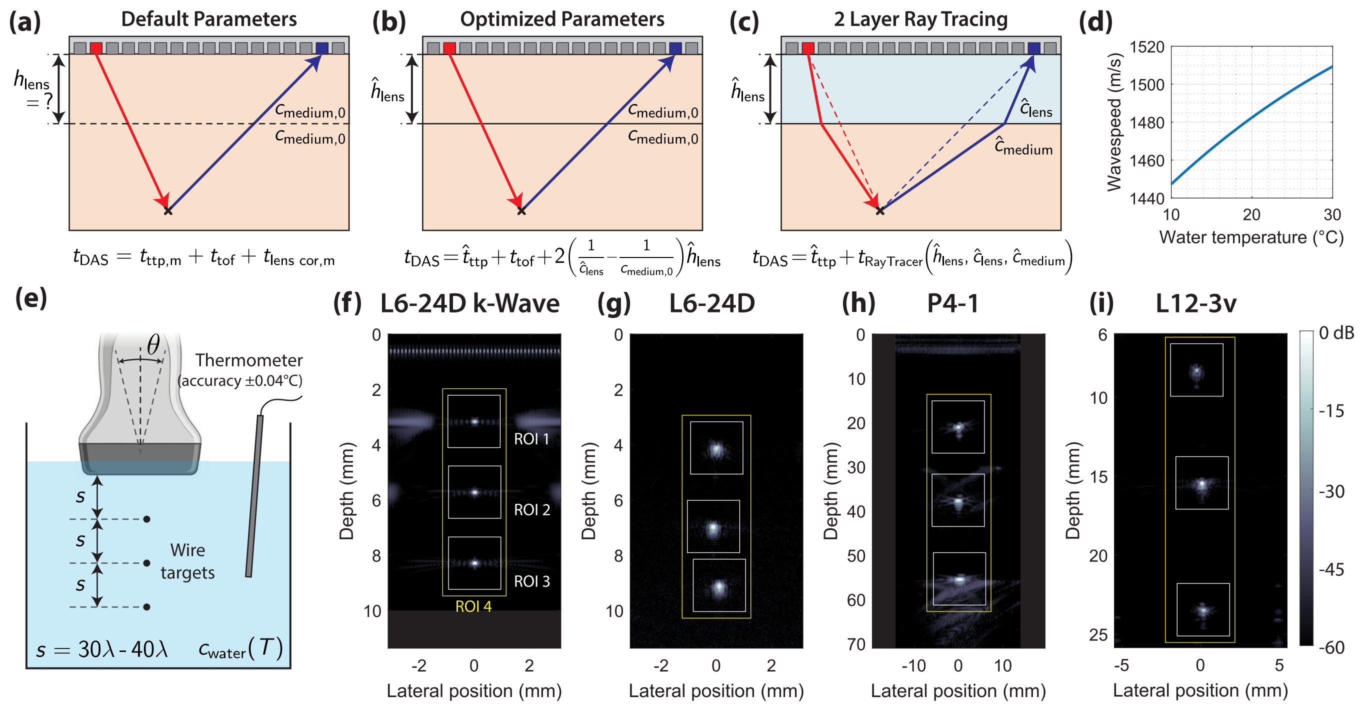

Fig. 2. Validation of the calibrated transducer parameters. (a) Conventional DAS image reconstruction using uncalibrated transducer parameters, called "default parameters" in this work. (b) "Default parameters" reconstruction approach using calibrated transducer parameters. (c) "Two-layer ray-tracing" reconstruction approach using calibrated transducer parameters. (d) Temperature of the water was converted to the ground truth sound speed of the water by using a calibration curve as published in [12]. (e) Validation setup consisting of three thin wires at a vertical distance of 30λ–40λ submerged in water. The transducer position was slightly changed between each of the ten acquisition repeats. The temperature of the water was measured using a high-accuracy thermometer. (f)–(i) B-mode images reconstructed using the two-layer ray-tracing approach and the calibrated transducer parameters. In the images, four ROIs are defined, three around the individual wires, and a fourth larger ROI that contained all the wires.

For numerical stability and to minimize numerical dispersion, we used a small grid step ($\Delta x = 1.18$ µm) that corresponds to 80 grid points per wavelength in water and a Courant–Friedrichs–Lewy condition of 0.3. The thickness of the perfectly matched layer (PML) was set to four wavelengths in water. The element in the center of the array transmitted a four-cycle pulse centered at 15 MHz with a Hanning envelope. The numerically generated echo signals were decimated to four samples per period (same sampling rate as the experimental data). The simulated echo signals are shown in Fig. 1(c).

B. Validation of the Estimated Transducer Parameters

To validate the calibrated transducer parameters, we performed a sound speed estimation of water with known sound speed using an autofocusing approach [8], [10].

1) Image Reconstruction Approaches: Throughout this article, three image reconstruction approaches are compared. All reconstruction approaches rely on DAS beamforming [1]; however, the approaches differ in the calculation of the round-trip travel times t_{DAS}. In the following, subscript $_{,m}$ denotes a manufacturer reported variable, subscript $_{,0}$ denotes a literature value, and the circumflex $\hat{}$ denotes a variable calibrated with the proposed method.

a) Image reconstruction with default parameters: This approach is most prevalent and is schematically represented in Fig. 2(a). The travel time for DAS is given by the following equation:

$$t_{DAS} = t_{tof} + t_{ttp,m} + t_{lens\ cor,m}. \tag{3}$$

The first term t_{tof} is the round-trip travel time in the medium as if the lens did not exist. The round-trip travel time depends on the transmitter position, the receiver position, the coordinates of the image pixel, and the sound speed in the medium $c_{medium,0}$. This approach assumes a straight ultrasound ray between an array element and an image pixel. In this approach, typical literature medium sound speed will be used, e.g., 1480 m/s for water [14], [15]. The value for the time to peak $t_{ttp,m}$ will be taken as the estimated value provided by the scanner manufacturer. The lens correction term $t_{lens\ cor,m}$ is also taken from the manufacturer and corrects for the fact that the ultrasound wave travels through a lens layer with a lower speed of sound than the medium. Therefore, $t_{lens\ cor,m}$ does not represent the round-trip travel time through the lens, but rather the difference caused by underestimation of the round-trip travel time.

b) Image reconstruction with optimized parameters: In this approach [Fig. 2(b)], the travel time for DAS is given by the following equation:

$$t_{DAS} = t_{tof} + \hat{t}_{ttp} + \hat{t}_{lens\ cor} \tag{4}$$

with $\hat{t}_{ttp}$ the calibrated value for time to peak of the waveform. The calibrated round-trip lens correction term $\hat{t}_{lens\ cor}$ is defined by the following equation:

$$\hat{t}_{\text{lens cor}} = 2\left(\frac{1}{\hat{c}_{\text{lens}}} - \frac{1}{c_{\text{medium},0}}\right)\hat{h}_{\text{lens}} \tag{5}$$

where $\hat{c}_{\text{lens}}$ is the calibrated lens sound speed, $c_{\text{medium},0}$ is a literature value for the medium sound speed, and $\hat{h}_{\text{lens}}$ is the calibrated lens thickness. Like with the default parameters approach, this second approach assumes a straight ultrasound ray between an array element and an image pixel, and t_{tof} denotes the round-trip time of flight (TOF) as if the lens did not exist.

c) Image reconstruction with two-layer ray tracing: In this approach, two-layer ray tracing is used to account for the phase aberration caused by the transducer lens [Fig. 2(c)]. By using ray tracing, Snell's law of refraction is imposed on the lens–medium interface to find the refracted wave path. The first layer has a thickness $\hat{h}_{\text{lens}}$ and speed of sound $\hat{c}_{\text{lens}}$, and the second layer has a sound speed $\hat{c}_{\text{medium}}$. To find the refracted wave path, we perform two-point ray tracing using Fermat's principle [16]. The travel time is computed for every transducer element and image point pairs and used as an input for the DAS reconstruction algorithm. The travel time for DAS is given by the following equation:

$$t_{\text{DAS}} = \hat{t}_{\text{ttp}} + t_{\text{RayTracer}}\left(\hat{h}_{\text{lens}}, \hat{c}_{\text{lens}}, \hat{c}_{\text{medium}}\right) \tag{6}$$

with $\hat{t}_{\text{ttp}}$ the calibrated value for time to peak of the waveform, $\hat{c}_{\text{lens}}$ the calibrated lens sound speed, and $\hat{c}_{\text{medium}}$ the calibrated medium sound speed as found by autofocusing (Section II-B3). The round-trip travel time computed by the ray tracer $t_{\text{RayTracer}}$ inherently includes the travel time through the lens and in the scanned medium. The ray-tracing algorithm is described in detail in [8].

2) Experimental Setup and Data Acquisition: A tank with an acoustic absorbing layer at the bottom was filled with pure water (milli-Q). In this tank, we submerged a phantom with three vertically positioned wires, spaced with an interwire vertical distance of 30λ–40λ [see Fig. 2(e)]. The wire phantom for the P4-1 had 50 μm-diameter copper wires, for the L12-3v and the L6-24D nylon wires with a diameter of 10 μm were used. Next, the probe was positioned above the wires at a distance of 30λ–40λ, and the wires were imaged using a synthetic aperture sequence with single-element transmissions. The acquisition was repeated ten times, and in each trial, the angle of the probe in the imaging plane was slightly varied.

At the start and end of the imaging session, the temperature of the water was measured with a high-accuracy thermometer (PT100 thermocouple, accuracy ±0.04 °C, Greisinger electronics, Germany). To obtain the ground truth sound speed of the water, the temperature was converted to sound speed using a calibration curve [Fig. 2(d)] [12].

3) Estimation of the Sound Speed of the Medium Using Autofocus: The sound speed of water was estimated using autofocusing [8], [10]. To start, an initial reconstruction using the two-layer ray-tracing approach with an initial estimate of the sound speed $c_{\text{medium},0} = 1480$ m/s was done. In the images, the locations of the three wires were detected using peak finding, and around the center of each wire, a $20\lambda \times 20\lambda$ region of interest (ROI) was defined [see Fig. 2(f)–(i)]. A fourth ROI that contained all wires was defined.

Autofocusing was done per ROI and for each acquisition repeat. The sound speed was estimated by reconstructing an ROI with a range of speed of sound values and computing a focus quality metric for each tested value. During image reconstruction for autofocusing purposes, it is important to use the largest aperture possible. As a focus metric, a combination of the image intensity and two metrics of image sharpness was used as validated before in [8] and [10]. The intensity of the ROI image was calculated as the sum of the squared amplitude of the image envelope. The sharpness was assessed with two metrics, the Brenner gradient and the normalized variance [10]. Each focus metric was individually normalized by dividing by the maximum value, and the three normalized focus metrics were summed with equal weights to compute focus quality. The estimated water sound speed $\hat{c}_{\text{medium}}$ is the value that maximizes focus quality.

4) Impact of Transducer Lens Correction on Image Quality: To assess the impact of the lens on B-mode imaging, we compared images of the wire targets using the three reconstruction approaches. Images were reconstructed with F-number 2.0. We assessed the axial and lateral resolutions using the full-width at half-maximum (FWHM) of the point spread function (PSF). We assessed the contrast of the PSFs using the cystic resolution [17]. The cystic resolution is used to quantify the capacity for detecting an anechoic cyst within a uniformly scattering medium. It is defined as the ratio of energy outside a circular region centered around the PSF with radius r, normalized by the total energy of the PSF

$$C(r) = 10 \log \sqrt{\frac{E_{\text{out}}(r)}{E_{\text{total}}}}. \tag{7}$$

To obtain a single metric from the $C(r)$-curve, you can find the relative intensity for a particular cyst size or determine the size needed to reach a specific relative energy. In this study, contrast is assessed using a fixed radius of 2.5 ultrasound wavelengths [18].

5) Simulation of the Effect of Lens Correction as a Function of Depth: To assess the impact of accurate transducer lens parameters on sound speed retrieval and image quality, we simulated the acquisition of echo signals backscattered by three small targets with the L6-24D transducer using the numerical wave solver k-Wave [13]. The simulation parameters are described in Section II-A3. Below the lens layer, we defined a layer of water with a sound speed of 1480 m/s and a density of $1000\,\text{kg/m}^3$. We modeled three wire targets with a diameter ten times smaller than the wavelength submerged in water at three depths corresponding to 40, 80, and 120 ultrasound wavelengths. We simulated an element-by-element transmission scheme for synthetic aperture imaging. The echo signals were decimated to obtain a sampling frequency of $4 f_{\text{tx}}$ (such as the experimental data), where f_{tx} is the ultrasound transmit frequency.

The optimized parameters and two-layer ray-tracing approaches were used to estimate the sound speed in the simulated water layer. The sound speed was estimated using the autofocusing approach described in Section II-B3. The

TABLE II
ESTIMATED TRANSDUCER PARAMETERS USING THE PROPOSED METHOD

		L6-24D k-Wave	L6-24D	P4-1	L12-3v
$\hat{c}_{\text{lens}}$	(m/s)	997.0	1015.2	924.7	1009.6
$\hat{h}_{\text{lens}}$	(mm)	0.600	0.615	1.236	0.663
$\hat{t}_{\text{ttp}}$	(ns)	166.5	331.8	742.9	486.9
$\hat{t}_{\text{lens cor}}$	(μs)	0.39	0.38	1.00	0.42

calibrated sound speed was compared to the ground truth sound speed of water. Next, we reconstructed b-mode images and assessed the image quality in terms of resolution and contrast, described in detail in Section II-B4.

III. RESULTS

A. Calibration of Transducer Parameters

1) Simulation Results: We used the k-Wave simulation of the internal lens reflections [Fig. 1(c)] to validate our proposed method. In simulation, no multiple reflections are visible in the echo signals since we modeled a semi-infinite medium. The coherence score for the tested values of lens thickness, lens sound speed, and time to peak in the grid search is shown in Fig. 1(e)–(g). The estimated transducer parameters are shown in Table II. The error for the retrieved parameters was 3.03 m/s for the lens sound speed, below 0.1 µm for the lens thickness, and 0.71 ns for the time to peak.

2) Experimental Results: We calibrated the three transducer parameters using the proposed method. The echo signals and the results of the parameter optimization for all three transducers are shown in Fig. 3. The estimated transducer parameters can be found in Table II.

B. Validation of Estimated Transducer Parameters With Autofocusing in Water

We validated transducer lens parameters estimated in simulation and experimentally by performing autofocusing with the two-layer ray-tracing reconstruction approach in a water medium with a known speed of sound.

1) Simulation: In the simulation, the ground truth water sound speed was 1480 m/s. The results for autofocusing with the optimized parameters reconstruction and the two-layer ray-tracing reconstruction are shown in Fig. 4(a). An error of up to 45 m/s is obtained with the optimized parameters reconstruction, while the two-layer ray-tracing reconstruction provides an error smaller than 0.5 m/s (Table III).

2) Experiment: Experimentally, we measured the temperature of the water with a high-precision thermometer. For experiments with P4-1, we measured a temperature of 20.88 °C, for the L12-3v we measured 20.91 °C and for the L6-24D we measured 21.71 °C. The measured temperatures corresponded to a ground truth sound speed in water of 1485.14 m/s for P4-1, 1485.23 m/s for L12-3v, and 1487.61 m/s for L6-24D.

TABLE III
MEAN (STANDARD DEVIATION) ERROR IN ESTIMATED WATER SOUND SPEED (M/S), FOUND BY AUTOFOCUSING USING THE THREE DIFFERENT RECONSTRUCTION APPROACHES. NEGATIVE NUMBERS INDICATE UNDERESTIMATION. WE COMPARE THE ERROR FOR THE DIFFERENT ROI DEFINED IN FIG. 2

		Speed of sound error (m/s)		
		Default Parameters	Optimized Parameters	2 Layer Ray Tracing
L6-24D k-Wave	ROI 1		-46.7	0.5
	ROI 2		-25.5	0.2
	ROI 3		-17.2	0.3
	ROI 4		-44.5	0.5
L6-24D	ROI 1		-37.4 (5.2)	2.4 (1.4)
	ROI 2		-20.9 (2.4)	0.9 (0.2)
	ROI 3		-16.1 (1.4)	0.7 (0.3)
	ROI 4		-33.7 (5.5)	2.3 (1.3)
P4-1	ROI 1	41.9 (1.7)	-16.8 (0.9)	-1.3 (1.1)
	ROI 2	18.8 (0.6)	-14.5 (0.8)	-6.5 (0.6)
	ROI 3	6.5 (3.0)	-15.3 (2.9)	-10.3 (2.8)
	ROI 4	41.7 (1.6)	-17.1 (1.6)	-1.4 (1.2)
L12-3v	ROI 1	42.8 (1.9)	17.2 (0.4)	3.5 (0.8)
	ROI 2	22.8 (0.7)	10.6 (0.3)	1.0 (0.4)
	ROI 3	15.9 (0.3)	6.8 (0.3)	0.8 (0.3)
	ROI 4	23.8 (0.9)	11.1 (0.4)	1.4 (0.6)

Because lens properties for the L6-24D are not provided by the manufacturer, we only compared image reconstruction with optimized parameters to image reconstruction with two-layer ray tracing.

Fig. 4 shows the result for autofocusing with the three approaches per ROI. For ROI 1, it is clear that for all transducers, the two-layer ray-tracing reconstruction provides the estimates that are closer to the ground truth sound speed. Table III shows the error in sound speed for all transducers and the three reconstruction approaches. The optimized parameters reconstruction underestimates the water sound speed for every ROI. For P4-1 and L12-3v, the default parameters reconstruction overestimates the water sound speed for every ROI. The most accurate sound speed estimation is obtained with the two-layer ray-tracing reconstruction, and the corresponding small error (<10 m/s) is nearly independent of depth. In contrast, the error in estimated sound speed increases as depth decreases (up to 41 m/s error) for the default parameters and optimized parameters reconstruction approaches.

C. Accurate Estimation of Transducer Parameters Improves Image Quality

After optimizing the transducer parameters and retrieval of the water sound speed with autofocus, we characterized the resolution and contrast for the wire PSFs. In the default parameters and optimized parameters reconstruction approaches, we reconstructed the images of the wire with a literature value for the sound speed of water at 20 °C, i.e., $c_{\text{water},0} = 1480$ m/s. For the two-layer ray-tracing reconstruction, we used the result of autofocusing for ROI 4.

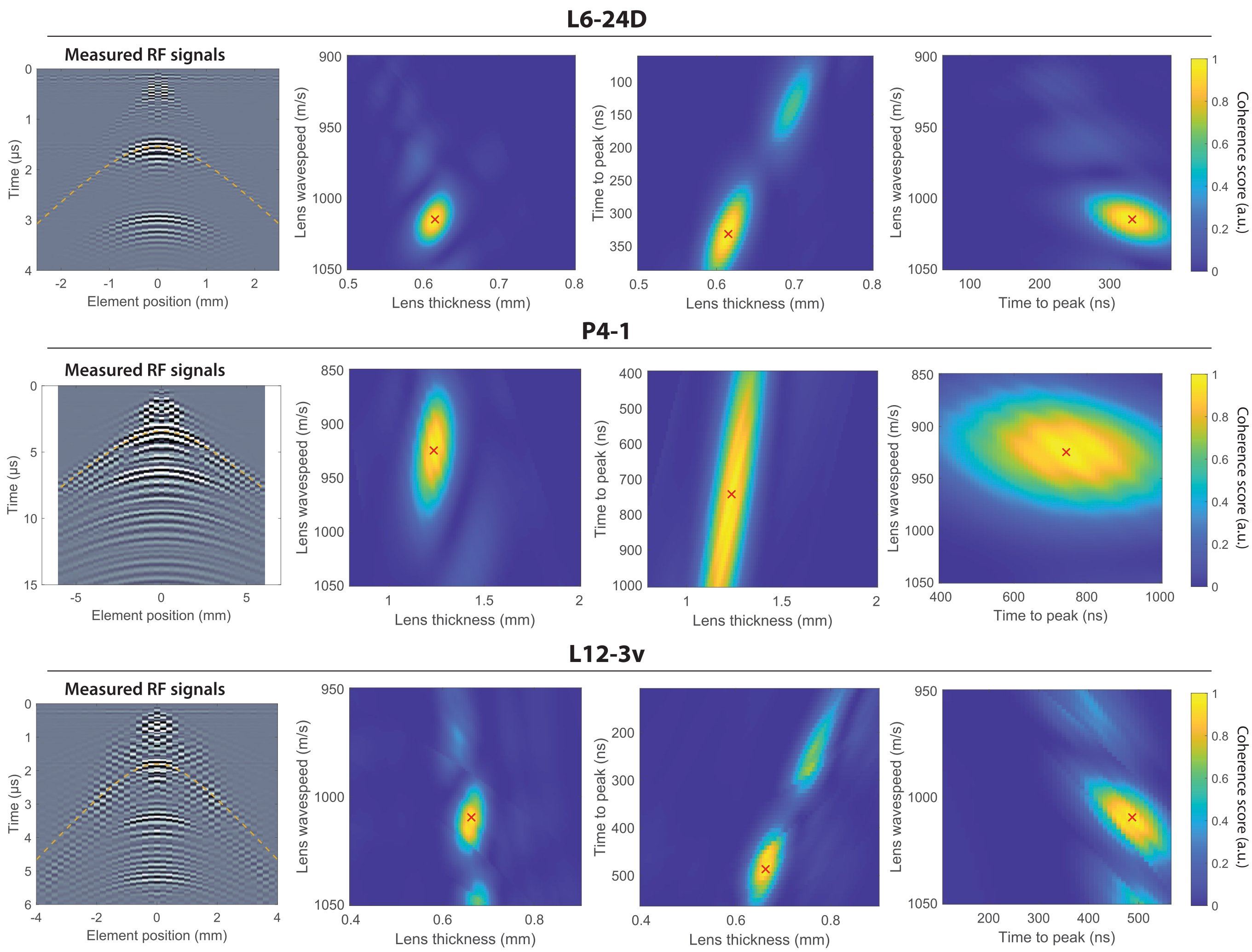

Fig. 3. Normalized coherence of the RF along the travel time hyperbolas for different tested values for lens thickness, lens sound speed, and time to peak in the grid search. The estimated transducer parameters are indicated by the red cross.

Fig. 5 depicts the largest improvement in lateral resolution (up to a twofold improvement) and contrast (up to 4 dB improvement) observed in ROI 1, i.e., with the wire that is the closest to the transducer (depth = 30–40 ultrasound wavelengths). The detailed characterization of the resolution and contrast for all wires is shown in Table IV. Table IV shows that the improvement in resolution and contrast is depth dependent, and the improvement is the largest for the shallow targets. As expected, mild variations in axial resolution were measured (Fig. 5 and Table IV) since axial resolution is essentially determined by the temporal duration of the ultrasound pulse.

IV. Discussion

A. Importance of the Lens Thickness

The smallest improvement in image quality was achieved with the P4-1 and the largest improvement with the L6-24D. This is due to the difference in relative lens thickness (in terms of ultrasound wavelengths). The lens thickness was found to be close to two wavelengths for P4-1, 4.5 wavelengths for L12-3v, and 6.5 wavelengths for L6-24D. The thicker the lens (in wavelengths), the stronger the effect of the lens. Therefore, transducers with thick lenses will benefit the most from the two-layer ray-tracing reconstruction.

The default parameters reconstruction overestimated sound speed in water. This is because the estimated lens correction provided by the scanner manufacturer was largely overestimating the lens thickness (Tables I and II). During autofocusing, the overestimation of the travel time in the lens causes an overestimation of the sound speed in water.

B. Shape of the Lens and Effective Lens Thickness

Silicone rubber lenses most often have either a weakly (cardiac phased-array transducers such as the P4-1) or a more pronounced convex shape (linear array transducers such as L6-24D and L12-3v) to produce elevational focusing. If the lens is flat, our approach estimates the true lens thickness. If the lens has curvature, our approach estimates an effective lens thickness. The validation using autofocusing in water demonstrates that for a wide range of lens curvatures, the lens is well approximated by a flat lens with an effective thickness.

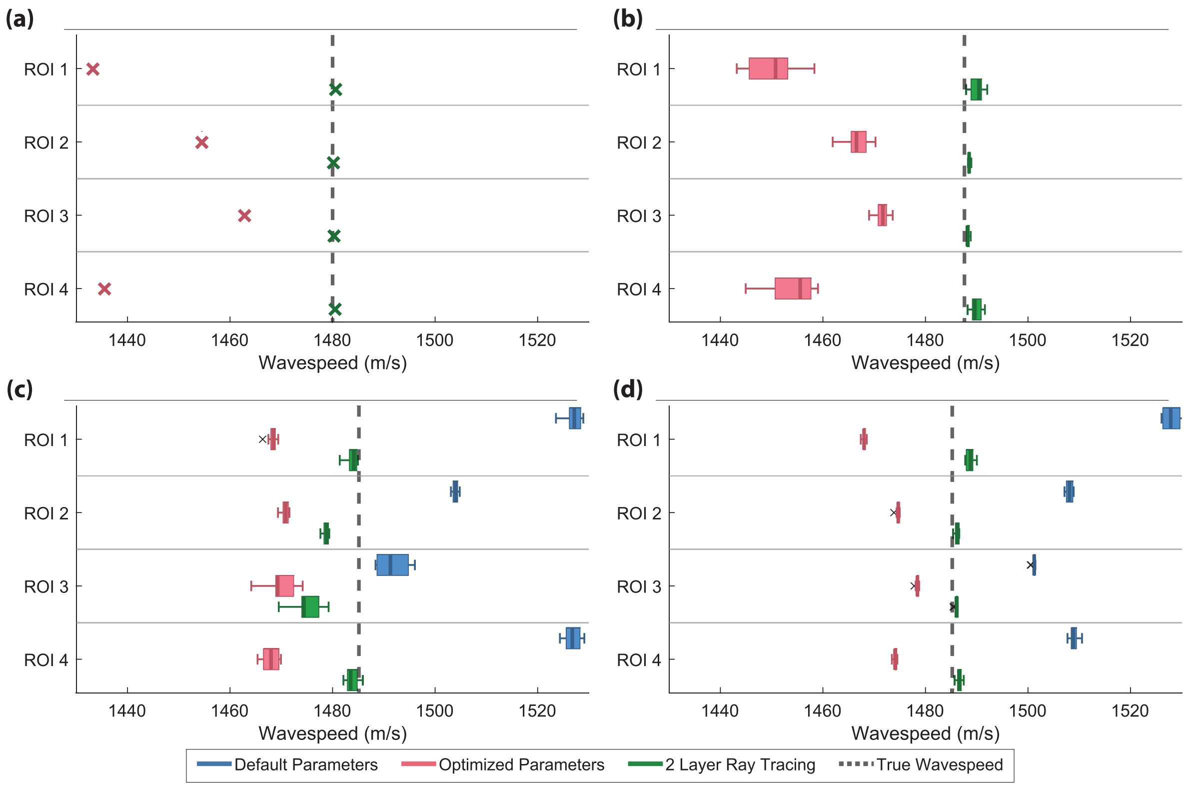

Fig. 4. Result of autofocusing to find the sound speed of water for the four different ROIs. We compare the result of autofocusing for the three reconstruction approaches. For the physical transducers, the boxplots indicate the statistics over the ten acquisition repeats. For the simulated transducer, no statistics are available. Gray dashed line indicates the ground truth water sound speed as obtained by temperature measurement. (a) Results of autofocusing for the simulated L6-24D transducer. (b) Results of autofocusing for the L6-24D. (c) P4-1. (d) L12-3v.

TABLE IV
DETAILED RESULTS OF PSF CHARACTERIZATION FOR ALL THREE WIRES. THE RESULTS ARE SHOWN AS MEAN (STANDARD DEVIATION)

		Lateral resolution (μm)			Axial resolution (μm)			Contrast (dB)		
		Default	Optimized	2L Ray	Default	Optimized	2L Ray	Default	Optimized	2L Ray
L6-24D k-Wave	ROI 1		146.4	123.6		82.4	77.2		-23.3	-24.6
	ROI 2		149.2	114.2		83.4	74.8		-29.0	-31.0
	ROI 3		136.0	107.1		81.5	78.2		-31.3	-33.9
L6-24D	ROI 1		198.2 (17.9)	114.6 (3.7)		117.0 (4.9)	111.1 (11.8)		-18.8 (3.4)	-23.6 (2.0)
	ROI 2		148.1 (9.5)	114.1 (4.0)		117.0 (14.3)	116.9 (16.5)		-24.2 (1.6)	-26.2 (1.7)
	ROI 3		137.0 (6.3)	123.1 (2.9)		123.7 (12.4)	131.8 (19.8)		-24.1 (2.0)	-25.1 (1.9)
P4-1	ROI 1	867.5 (51.1)	604.9 (16.6)	585.9 (16.5)	520.8 (16.0)	520.5 (12.4)	522.0 (10.4)	-25.2 (0.8)	-27.7 (1.0)	-27.7 (1.0)
	ROI 2	872.5 (23.6)	867.8 (7.2)	863.6 (9.7)	520.2 (10.3)	510.7 (12.8)	511.3 (11.4)	-22.8 (0.9)	-23.9 (0.8)	-23.8 (0.9)
	ROI 3	1087.5 (25.9)	1092.5 (35.8)	1090.1 (38.6)	524.1 (8.8)	522.3 (11.6)	524.6 (12.1)	-21.1 (0.6)	-21.3 (0.6)	-21.3 (0.6)
L12-3v	ROI 1	477.7 (16.7)	263.3 (11.4)	164.4 (4.8)	144.4 (5.4)	167.5 (6.4)	160.1 (5.1)	-17.8 (0.7)	-20.9 (0.8)	-21.8 (0.8)
	ROI 2	356.3 (18.2)	221.3 (5.8)	189.0 (2.8)	149.0 (1.9)	155.5 (1.3)	160.2 (3.3)	-24.6 (0.7)	-27.2 (0.7)	-27.9 (0.4)
	ROI 3	281.3 (20.3)	229.2 (7.3)	220.6 (7.0)	151.6 (10.4)	153.5 (11.1)	155.8 (11.0)	-21.4 (2.1)	-23.4 (2.4)	-23.8 (2.4)

C. Advantages of Air-Coupled Acquisition for the Estimation of Transducer Parameters

Using air as a coupling medium to record internal reflections in the lens has multiple advantages. Thanks to the high acoustic impedance contrast, the echo signals reflected at the interface between the silicone rubber of the lens and air have sufficient amplitude. Using a liquid like water is not advantageous because there would exist a critical angle $\theta_c = \arcsin(c_{\text{lens}}/c_{\text{water}}) = 42.5°$. Part of the wavefront emitted by a single transducer element would experience supercritical reflection at the interface between the lens and the fluid. As a consequence, a phase shift would occur in part of the reflected wavefront. This phase shift would bias the coherence metric. In addition, a measurement in air is simpler and quicker than a measurement in a liquid.

Although designed for scattering from a medium containing small heterogeneities, methods proposed for sound speed

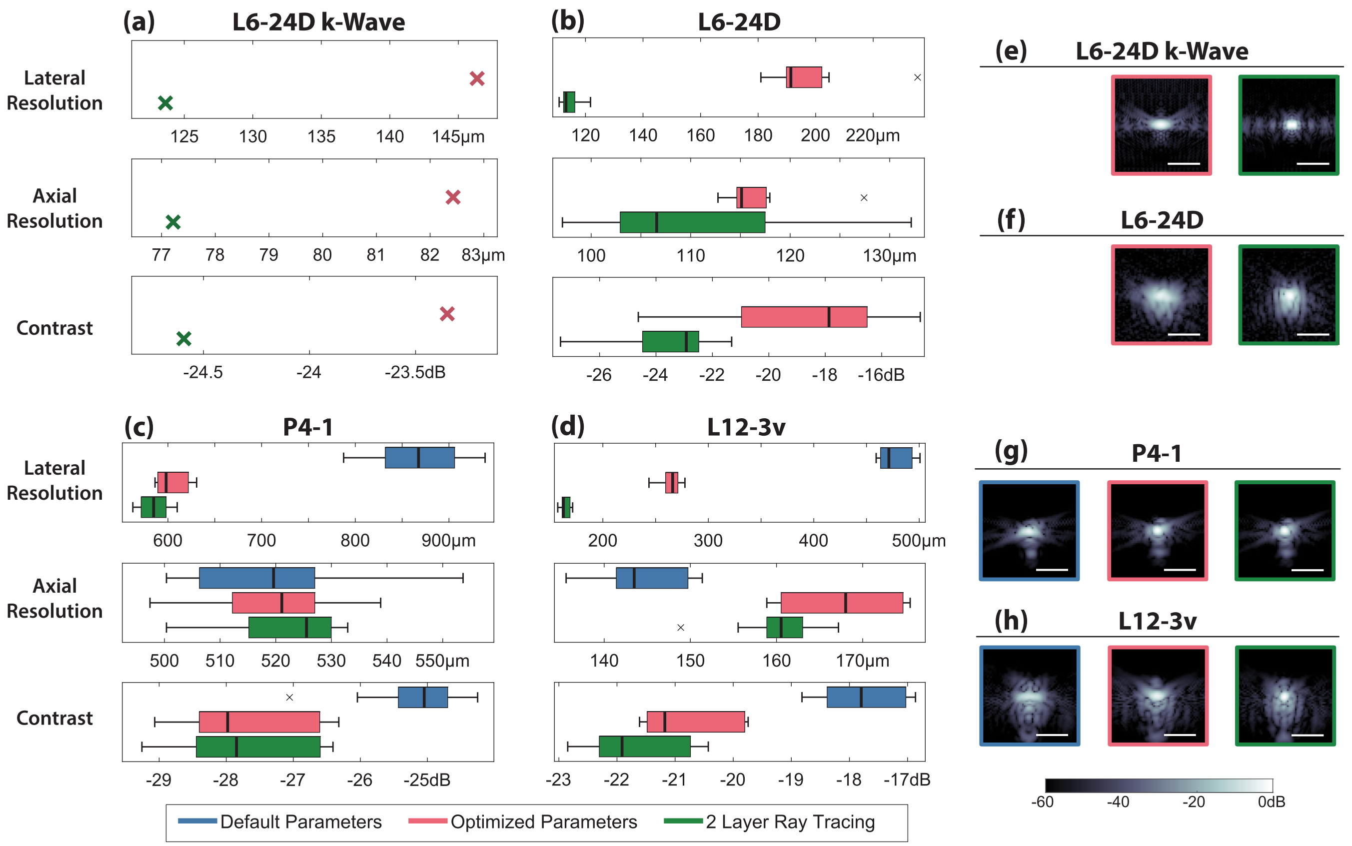

Fig. 5. (a)–(d) Results of PSF characterization for each transducer. All shown results are for the wire in ROI 1 [see Fig. 2(f)–(i)]. We compared the image quality of the three reconstruction approaches. Lateral and axial resolutions were determined using the FWHM. Contrast was determined using the cystic resolution [17]. (e)–(h) Zoom of the PSF of the wire in ROI 1. The PSF is shown for the three approaches, the PSF surrounded by the blue rectangle is obtained by reconstruction with the default parameters, the PSF in the red rectangle is obtained using the optimized parameters, and the PSF in the green rectangle is obtained by two-layer ray tracing. Scale bars denote five wavelengths.

estimation in the scanned medium [19], [20], [21] could be potentially adapted to the estimation of the sound speed in the lens of the transducer and applied to air-coupled data acquisition. However, these methods would not provide an accurate estimate of the lens thickness and do not estimate the time to peak of the ultrasound waveform.

D. Different Components in the Estimated Time to Peak

The time-to-peak parameters estimated with the proposed method contain actually three components: 1) the actual time to peak of the backscattered ultrasound pulse; 2) the two-way travel time in the matching layers (a diced matching layer only causes a delay); and 3) any time lag caused by the scanner during transmit and receive. It is worth mentioning that the true time to peak of the backscattered ultrasound pulse is determined by the electric excitation waveform. Therefore, it is advised to perform the proposed calibration of the transducer parameters every time the electric excitation waveform is modified.

E. Challenges in Estimation of Transducer Parameters

When the internal specular reflection in the lens is clearly recorded, the estimation of transducer parameters is straightforward, such as for the simulated and experimentally acquired L6-24D data (Fig. 1). Transducers with less advanced design and poorer manufacturing quality may produce internal reflection signals of poor quality because guided waves inside the different layers in the transducer may generate signals with an amplitude similar to that of the internal specular reflection in the lens. Fig. 3 shows that the L12-3v and the P4-1 transducers produce internal reflection signals that are more challenging to exploit for estimating the transducer parameters. When the signal quality is insufficient, it is possible to extend the method by using both the primary and secondary (two round trips in the lens) reflections. To construct the arrival time hyperbola of the secondary reflection, the round-trip travel time through the lens is determined using the following equation:

$$\tau_{\text{rt-2}}(x_{\text{tx}}, x_{\text{rx}}) = \frac{4}{c_{\text{lens}}}\sqrt{\left(\frac{x_{\text{tx}} - x_{\text{rx}}}{4}\right)^2 + h_{\text{lens}}{}^2} \tag{8}$$

where x_{tx} is the lateral coordinate of the transmitting element and x_{rx} is the lateral coordinate of the receiving element. Finally, the TOF hyperbola can be constructed by adding the time to peak to $\tau_{\text{rt-2}}$ and a correction term for the round-trip propagation time through the matching layers t_{ml}. An ultrasound transducer possesses often two matching layers. The thickness of a matching layer is one-quarter wavelength, and therefore, the round-trip travel time through the matching layers is $t_{\text{ml}} = (1/f_c)$, where f_c is the center ultrasound

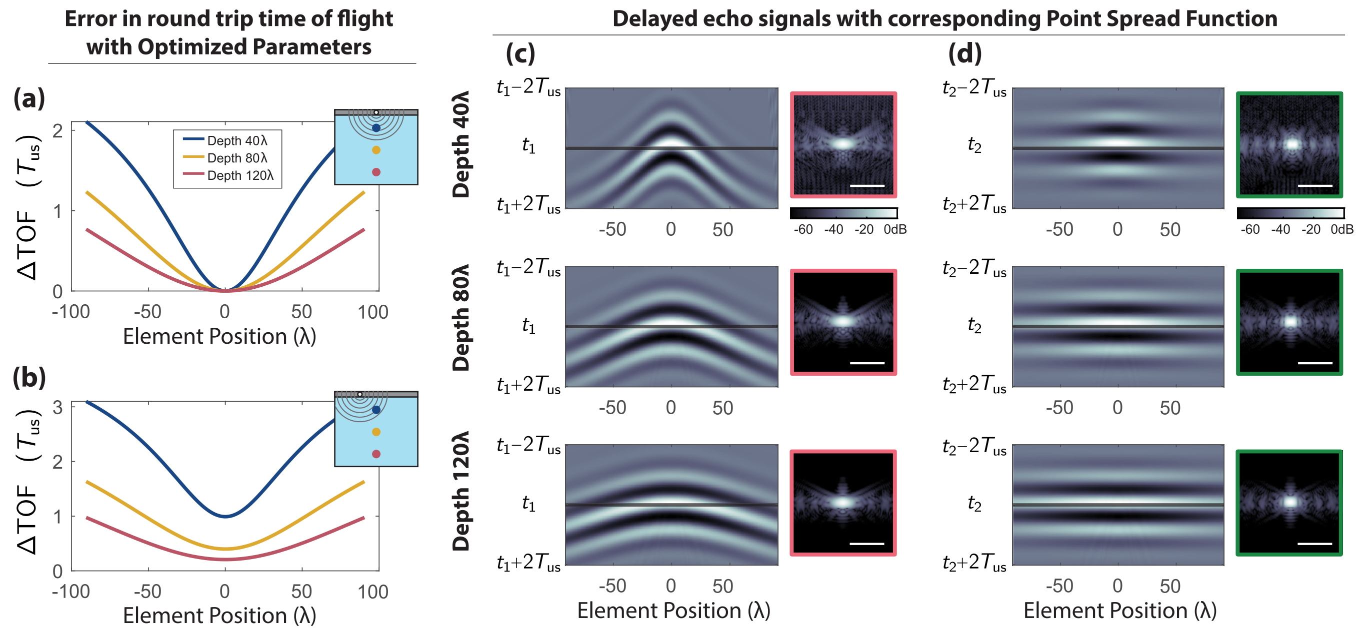

Fig. 6. Investigating the impact of lens correction on the estimated round-trip TOF with the *k*-Wave simulation of the L6-24 transducer. Difference in the estimated round-trip TOF (ΔTOF) between the optimized parameters and the two-layer ray-tracing reconstruction approaches if (a) source is located directly above the targets and if (b) source is located at -40λ lateral distance from the targets. ΔTOF is presented in units of the ultrasound wave period $T_{us} = 1/f_{tx}$. The TOF computed using two-layer ray tracing can be considered the ground truth. (c) TOF is computed using the optimized parameters for the three wire targets, given by the hyperbola t_1. When delaying the echo signals using TOF hyperbola t_1, it becomes clear that the TOF is underestimated for all wire targets since the echo signals do not line up with t_1. Signals are displayed in a temporal window of $t_1 \pm 2T_{us}$. The corresponding PSF for each imaging depth is shown right of the echo signals. The scale bar corresponds to five wavelengths in water. (d) When the TOF is computed using two-layer ray tracing, resulting in hyperbola t_2, the delayed echo signals line up perfectly with t_2 for all wire targets.

frequency of the transducer frequency bandwidth (calculation at normal incidence, a valid assumption if the matching layers are diced).

F. Depth Dependence of Sound Speed Estimation

The estimated sound speed in water was nearly independent of the target depth with the two-layer ray-tracing reconstruction approach (Fig. 4), unlike with the other two reconstruction methods. This is due to the fact that for shallow targets, the ultrasound ray angle (defined from the normal at the transducer surface) in the lens is larger, and thus, ignoring wave refraction causes a significant error in the travel times. The same depth dependence is visible in the image quality improvements (Table IV). The biggest improvement for image resolution and contrast was made for the superficial targets (depth 30λ–40λ). For deeper targets, the image quality remains the same.

To explain the depth dependence, we took a closer look at the *k*-Wave simulation. We consider the TOF obtained with two-layer ray tracing the true TOF, as it accounts for the speed of sound difference between the lens and water and accounts for refraction. Comparing the TOF of the optimized parameters and two-layer ray tracing, we see that there is a substantial difference between the two [Fig. 6(a) and (b)]. When the source is located directly above the wire targets, the difference between the two methods is 0 for every depth for the transducer element above the targets since the path through the lens is straight and no refraction occurs. For the neighboring elements, the path is refracted, and the error in round-trip TOF increases rapidly with increasing lateral distance. For the deeper targets, the error in round-trip TOF is smaller since the ray angles become smaller. When a source is located at a lateral distance of the target, the optimized parameter reconstruction underestimated the TOFs for all elements.

The underestimation of the round-trip TOF is very apparent when overlaying the hyperbolas of the two methods on the echo signals or, alternatively, when the echo signals are delayed by the TOFs, as depicted in Fig. 6(c) and (d). The underestimation of the TOF explains why the speed of sound estimation with autofocusing consistently underestimated the true water sound speed. By using a lower speed of sound in water, the TOF is increased, and the echo signals line up better with the arrival time hyperbola. When using the correct transducer parameters in conjunction with two-layer ray tracing, the echo signals line up perfectly with the hyperbola regardless of target depth [Fig. 6(d)].

G. Considerations When Using Sound Speed as a Biomarker

The field of sound speed imaging aims to use sound speed as a potential biomarker to discriminate between healthy versus diseased tissue [22]. For instance, the difference in sound speed between healthy liver tissue and tissue with advanced steatosis is close to 100 m/s or less [23]. It is even more difficult to discriminate between different stages of steatosis since the difference in sound speed is in the order of tens of meters per second [24].

Our results indicate that both reconstruction algorithm and transducer parameters have a large influence on the retrieved medium sound speed. Although the ground truth sound speed for all experiments was very close, around 1486 $\pm$ 2 m/s, we retrieved the speed of sound values ranging from 1450 to 1525 m/s (Fig. 4). This indicates that results from various studies with different scanners, transducers, and sound speed retrieval methodologies are difficult to compare and highlight the need for technical standardization in order to use sound speed as a reliable biomarker [25].

V. Conclusion

We described a simple, nondestructive method to estimate the transducer lens thickness, the transducer lens sound speed, and the time to peak of the backscattered ultrasound pulse. We demonstrated that the combination of calibrated transducer parameters with a two-layer ray-tracing reconstruction approach enables accurate sound speed estimation and improves ultrasound image resolution and contrast up to a depth of 100 wavelengths, across the medical ultrasound frequency range.

Acknowledgment

The authors would like to thank Henry den Bok for his support in making wire phantoms and Nico de Jong for the valuable discussions.

References

[1] V. Perrot, M. Polichetti, F. Varray, and D. Garcia, "So you think you can DAS? A viewpoint on delay-and-sum beamforming," *Ultrasonics*, vol. 111, Mar. 2021, Art. no. 106309.

[2] K. K. Shung and M. Zippuro, "Ultrasonic transducers and arrays," *IEEE Eng. Med. Biol. Mag.*, vol. 15, no. 6, pp. 20–30, Nov. 1996.

[3] H. Favre, M. Pernot, M. Tanter, and C. Papadacci, "Transcranial 3D ultrasound localization microscopy using a large element matrix array with a multi-lens diffracting layer: An in vitro study," *Phys. Med. Biol.*, vol. 68, no. 7, Apr. 2023, Art. no. 075003.

[4] M. D. Gray and C. C. Coussios, "Compensation of array lens effects for improved co-registration of passive acoustic mapping and B-mode images for cavitation monitoring," *J. Acoust. Soc. Amer.*, vol. 146, no. 1, pp. EL78–EL84, Jul. 2019.

[5] J. A. Jensen, S. I. Nikolov, K. L. Gammelmark, and M. H. Pedersen, "Synthetic aperture ultrasound imaging," *Ultrasonics*, vol. 44, pp. e5–e15, Dec. 2006.

[6] M. E. Anderson, M. S. McKeag, and G. E. Trahey, "The impact of sound speed errors on medical ultrasound imaging," *J. Acoust. Soc. Amer.*, vol. 107, no. 6, pp. 3540–3548, Jun. 2000.

[7] J. F. Krucker, J. B. Fowlkes, and P. L. Carson, "Sound speed estimation using automatic ultrasound image registration," *IEEE Trans. Ultrason., Ferroelectr., Freq. Control*, vol. 51, no. 9, pp. 1095–1106, Sep. 2004.

[8] G. Renaud, P. Kruizinga, D. Cassereau, and P. Laugier, "In vivo ultrasound imaging of the bone cortex," *Phys. Med. Biol.*, vol. 63, no. 12, Jun. 2018, Art. no. 125010.

[9] G. Renaud, P. Clouzet, D. Cassereau, and M. Talmant, "Measuring anisotropy of elastic wave velocity with ultrasound imaging and an autofocus method: Application to cortical bone," *Phys. Med. Biol.*, vol. 65, no. 23, Nov. 2020, Art. no. 235016.

[10] B. E. Treeby, T. K. Varslot, E. Z. Zhang, J. G. Laufer, and P. C. Beard, "Automatic sound speed selection in photoacoustic image reconstruction using an autofocus approach," *J. Biomed. Opt.*, vol. 16, no. 9, 2011, Art. no. 090501.

[11] D. Napolitano et al., "Sound speed correction in ultrasound imaging," *Ultrasonics*, vol. 44, pp. e43–e46, Dec. 2006.

[12] W. Marczak, "Water as a standard in the measurements of speed of sound in liquids," *J. Acoust. Soc. Amer.*, vol. 102, no. 5, pp. 2776–2779, Nov. 1997.

[13] B. E. Treeby and B. T. Cox, "K-Wave: MATLAB toolbox for the simulation and reconstruction of photoacoustic wave fields," *Proc. SPIE*, vol. 15, no. 2, Mar. 2010, Art. no. 021314.

[14] P. N. T. Wells, *Biomedical Ultrasonics*. London, U.K.: Academic, 1977.

[15] C. M. Rumack, S. Wilson, J. W. Charboneau, and D. Levine, *Diagnostic Ultrasound, 2-Volume Set* Amsterdam, The Netherlands: Elsevier, 2010.

[16] D. A. Waltham, "Two-point ray tracing using Fermat's principle," *Geophys. J. Int.*, vol. 93, no. 3, pp. 575–582, Jun. 1988.

[17] K. Ranganathan and W. Walker, "Cystic resolution: A performance metric for ultrasound imaging systems," *IEEE Trans. Ultrason., Ferroelectr., Freq. Control*, vol. 54, no. 4, pp. 782–792, Apr. 2007.

[18] J. Jensen, M. B. Stuart, and J. A. Jensen, "Optimized plane wave imaging for fast and high-quality ultrasound imaging," *IEEE Trans. Ultrason., Ferroelectr., Freq. Control*, vol. 63, no. 11, pp. 1922–1934, Nov. 2016.

[19] M. Jakovljevic, S. Hsieh, R. Ali, G. C. L. Kung, D. Hyun, and J. J. Dahl, "Local speed of sound estimation in tissue using pulse-echo ultrasound: Model-based approach," *J. Acoust. Soc. Amer.*, vol. 144, no. 1, pp. 254–266, Jul. 2018.

[20] H.-C. Shin, R. Prager, H. Gomersall, N. Kingsbury, G. Treece, and A. Gee, "Estimation of speed of sound in dual-layered media using medical ultrasound image deconvolution," *Ultrasonics*, vol. 50, no. 7, pp. 716–725, Jun. 2010.

[21] M. E. Anderson and G. E. Trahey, "The direct estimation of sound speed using pulse–echo ultrasound," *J. Acoust. Soc. Amer.*, vol. 104, no. 5, pp. 3099–3106, Nov. 1998.

[22] S. J. Sanabria, E. Ozkan, M. Rominger, and O. Goksel, "Spatial domain reconstruction for imaging speed-of-sound with pulse-echo ultrasound: Simulation and in vivo study," *Phys. Med. Biol.*, vol. 63, no. 21, Oct. 2018, Art. no. 215015.

[23] M. Imbault et al., "Robust sound speed estimation for ultrasound-based hepatic steatosis assessment," *Phys. Med. Biol.*, vol. 62, no. 9, pp. 3582–3598, May 2017.

[24] M. D. Burgio et al., "Ultrasonic adaptive sound speed estimation for the diagnosis and quantification of hepatic steatosis: A pilot study," *Ultraschall der Medizin, Eur. J. Ultrasound*, vol. 40, no. 6, pp. 722–733, Dec. 2019.

[25] D. T. Fetzer et al., "Pulse-echo quantitative U.S. biomarkers for liver steatosis: Toward technical standardization," *Radiology*, vol. 305, no. 2, pp. 265–276, Nov. 2022.